THE JOURNAL OF PHYSICAL CHEMISTRY A

Article

pubs.acs.org/JPCA

Structure–Property Relationship of Amplified Spontaneous Emission in Organic Semiconductor Materials: TPD, DPABP, and NPB

Zhaoxin Wu,*[,†] Lin Ma,[†] Peng Liu,[†] Caihua Zhou,[‡] Shuya Ning,[†] Ahmed El-Shafei,[§] Xiang Zhao,*[,‡] and Xun Hou[†]

[†]Key Laboratory of Photonics Technology for information, Key Laboratory for Physical Electronics and Devices of the Ministry of Education, School of Electronic and Information Engineering, Xi'an Jiaotong University, Xi'an 710049, P. R. China

[‡]School of Science, Xi'an Jiaotong University, Xi'an 710049, P. R. China

[§]Polymer and Color Chemistry Program, North Carolina State University, Raleigh, North Carolina 27695, United States

ABSTRACT: *N*,*N*′-Diphenyl-*N*,*N*′-bis(3-methylphenyl)-(1,1′-biphenyl)-4,4′-diamine (TPD) was demonstrated to be suitable for stimulated emission in doping and nondoping planar waveguide structure, but the mechanism for its lasing is of ambiguity. With the aim of providing a microsscopic picture for its lasing, we performed a combined experimental and theortical investigation of the absorption, photoluminescence (PL), and stimulated emission of TPD and other two similar molecules: 1,4-bis(diphenylamino)biphenyl (DPABP) and *N*,*N*′-diphenyl-*N*,*N*′-bis(1-naphthyl)-1,1′-biphenyl-4,4″-diamine (NPB). It was found that DPABP shows the same amplified spontaneous emission (ASE) characteristics as TPD, but NPB did not. In theory, density functional theory (DFT) and Franck–Condon Principle were used to analyze the molecular geometry in the electronic ground state as well as the optically excited state and the vibrational levels in electronic ground state, respectively. The calculation results show that for TPD and DPABP, several strongly elongated high-frequency modes (1199–1664 cm^{-1}) in the carbon rings contribute to the distinct first vibronic sideband in the PL spectra, which form an effective four-level system for lasing. For NPB, when the peripheral toluene or benzene is replaced with naphthyl, a number of strongly elongated low-frequency modes (11–689 cm^{-1}) deriving from naphthyl leads to a series of energy sublevels, which destroys the four-level system. Our results provided a new insight and better understanding into the lasing of organic molecules.

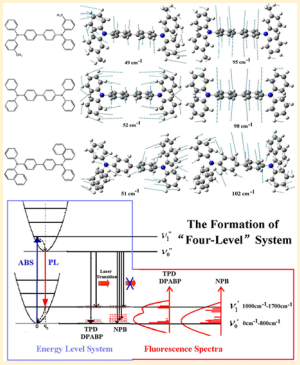

1. INTRODUCTION

Organic solid state lasing has received considerable attention in recent years. Because of the broad photoluminescence of organic materials, they are expected to be the promising candidates for solid state laser, which can be tuned over a wide wavelength range.[1−6] The main advantage of organic lasing materials is that their films can easily be fabricated by inexpensive and mild techniques, such as spin-coating, photolithography, inkjet printing, and vacuum thermal evaporation, in contrast with the sophisticated technology used with inorganic materials. *N*,*N*′-Diphenyl-*N*,*N*′-bis(3-methylphenyl)-(1,1′-biphenyl)-4,4′-diamine (TPD), as an attractive hole-transport material in organic light-emitting diode (OLED), has received considerable attention for its outstanding lasing characteristics.[7] It can be thermally evaporated, which provides an accurate control over the layer thickness and a better film quality. TPD was found to show stimulated emission at different concentrations (even in neat films). When doped at 30 wt % into polystyrene (PS), the amplified spontaneous emission (ASE) threshold of TPD film was the lowest reported to date in the lasing molecular materials.[7] As for the mechanism of lasing TPD, a few works were reported, and it was considered that the factors of Stokes shift, the radiative decay rate, the fluorescence lifetime, and the fluorescence quantum yield are correlated with the stimulated emission of TPD.[7−13] Up to now, however, from the molecular structure and energy level points of view, no theoretical explanations were proposed.

In this article, using samples as the TPD and other two similar molecules, 1,4-bis(diphenylamino)biphenyl (DPABP) and *N*,*N*′-diphenyl-*N*,*N*′-bis(1-naphthyl)-1,1′-biphenyl-4,4″-diamine (NPB), we investigated the effect of molecular structure and energy level on the stimulated emission in theory. In experiment, it was found that DPABP shows the same ASE characteristics as TPD, but NPB did not. Vibrational levels of the electronic ground state of the molecules in the present study was investigated by density functional theory (DFT) and by applying the Franck–Condon principle, which showed that, for TPD and DPABP, several strongly elongated high-frequency modes (1199–1664 cm^{-1}) in the aromatic rings result in obvious first vibrational sidebands in the PL spectra, which forms the four-level system for lasing. As for NPB, the replacement of the peripheral toluene or benzene with naphthyl leads to a number of strongly elongated low-frequency modes, which destroys the four-level system for lasing.

2. EXPERIMENTAL SECTION

2.1. Absorption, PL. TPD, DPABP, and NPB separately diluted in toluene solution containing polystyrene (PS) with 33 wt % were prepared and spin-coated over glass substrates. The structures of these molecules are shown in Figure 1. ABS and PL spectra were obtained by UV–vis spectrophotometer (HITACHI

Received: June 9, 2013
Revised: September 3, 2013
Published: September 13, 2013

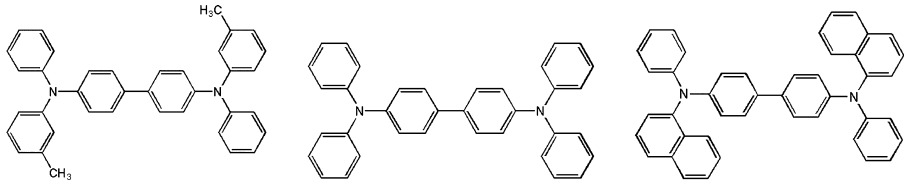

Figure 1. Molecular geometry of trans-isomer TPD, DPABP, and trans-isomer NPB.

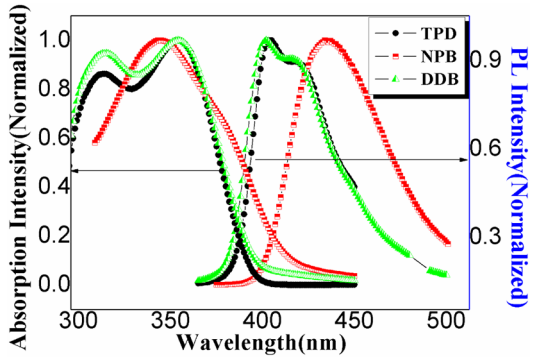

Figure 2. Optical absorption and emission spectra of three samples.

U-3010, Japan) and fluorescence spectrometer (fluoromax-4 spectrofluometer), respectively, and are shown Figure 2. PL spectra of TPD and DPABP consist of two main peaks: a main band with a maximum at around 404 nm and a first vibronic peak at around 424 nm, while NPB consists of a main band at 433 nm and no visible vibronic peak exists.

2.2. ASE Phenomenon. The experimental setup used to investigate the presence of stimulated emission in these organic materials has been reported elsewhere.[14−16] Shown in Figure 3,

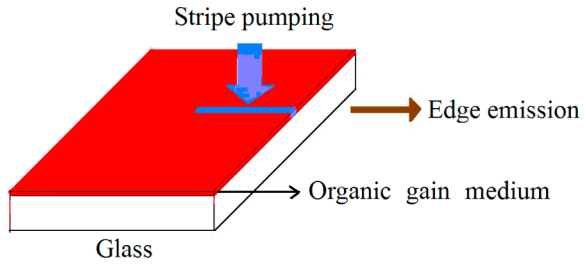

Figure 3. Schematic illustration of configuration of waveguide and excitation-detection.

samples were photopumped at normal incidence with a pulsed Nd:YAG laser (5.55 ns, 10 Hz) (Surelite I, Continuum Corp, USA) operating at 355 nm, which lies on the absorption region of the samples. Figure 4 shows ASE or emission characteristics of films of TPD, DPABP, and NPB. In Figure 4a,b, full widths at half-maximum (fwhm) of the emission spectrum of TPD decrease to 5 nm, and the output emission was amplified when the energy of pumped laser pulse was above the threshold. DPABP has the same ASE characteristics as TPD shown in Figure 4c,d. Shown as insets of Figure 4b,d, ASE takes place at the wavelength of the first vibronic peak of PL spectra. In contrast, the fwhm of NPB is around 75 nm, and there is no significant gain-narrowing even when the pump energy is at 8 mJ/cm^2 (Figure 4e,f), which exceeds the damage threshold of NPB film.The detail characteristics of ASE are shown in Table 1.

3. THEORETICAL ANALYSIS

The experiment results obviously showed lasing actions of TPD and DPABP films, but NPB did not. We analyzed the vibrational modes and PL spectra on the basis of the equilibrium molecular geometry by Gaussian09 program package based on density functional theory (DFT) and time-dependent DFT (TD-DFT). According to the calculation results, we illustrate the influence of vibrational modes for energy level system. Hence, we present here in the formation of a four-level system of small molecules, which is essential for lasing action, and elucidates the mechanism of lasing for TPD and DPABP.

3.1. Computational Methods. *3.1.1. Geometry Optimization.* The computational analysis only considers the single molecule for the following reasons. On one hand, it has reported that the intermolecular distances of TPD in the crystalline phase are large, without any evidence for stacking of the aromatic rings.[17] On the other hand, TPD diluted in PS as an inert polymer results in the large intermolecular distances, and it has ASE characteristics when optically pumped,[7] which indicates intermolecular interactions play a minor role in the photophysical property, especially ASE characteristics.

All DFT and TD-DFT calculations were carried out using the Gaussian09 program package. For TPD, DPABP, and NPB, the ground-state equilibrium molecular geometry using DFT calculation, were optimized using the functional B3LYP and the basis set 6-31g(d,p), and the TD-DFT method was applied to optimize the excited-state equilibrium molecular geometry by using the same functional and basis set. In the vertical excitation energy calculation, all excited states were obtained using TD-DFT in the adiabatic approximation,[16] using the same functional and basis set.

3.1.2. Calculation Model of the PL Spectra. In order to investigate the PL spectra of single TPD, DPABP, and NPB molecules, it is necessary to calculate the transition probability, which is related to the molecular structure. In the adiabatic approximation, the electronic ground and excited states wave functions can be expressed as the product of an electronic and nuclear part. When it assumes a single vibronic coordinate for simplicity, and neglecting any dependence of the electronic transition dipole moment on the nuclear position, the vibronic part of the total wave function contributes only to a Franck−Condon overlap factor. Restricting the discussion to the lowest vibronic level $|0_e\rangle$ of the first excited-state vibronic as the initial state, the probability to emit through a transition to the electronic ground state vibronic level $|n_g\rangle$ with an electric field E at energy E_L is given by Fermi's golden rule:[19]

$$P(|0_e\rangle \rightarrow |n_g\rangle) = \frac{2\pi}{\hbar} |\vec{E}\cdot\vec{\mu}|^2 |\langle 0_e|n_g\rangle|^2 \times \delta(E_L + E_{HOMO} - E_{LUMO} - n_e\hbar\omega) \quad (1\text{-}1)$$

In PL spectrum, for example, 0−0 transition means $|0_e\rangle \rightarrow |0_g\rangle$ transition, 0−1 transition means $|0_e\rangle \rightarrow |1_g\rangle$ transition, and μ is the

dx.doi.org/10.1021/jp405692c | J. Phys. Chem. A 2013, 117, 10903−10911

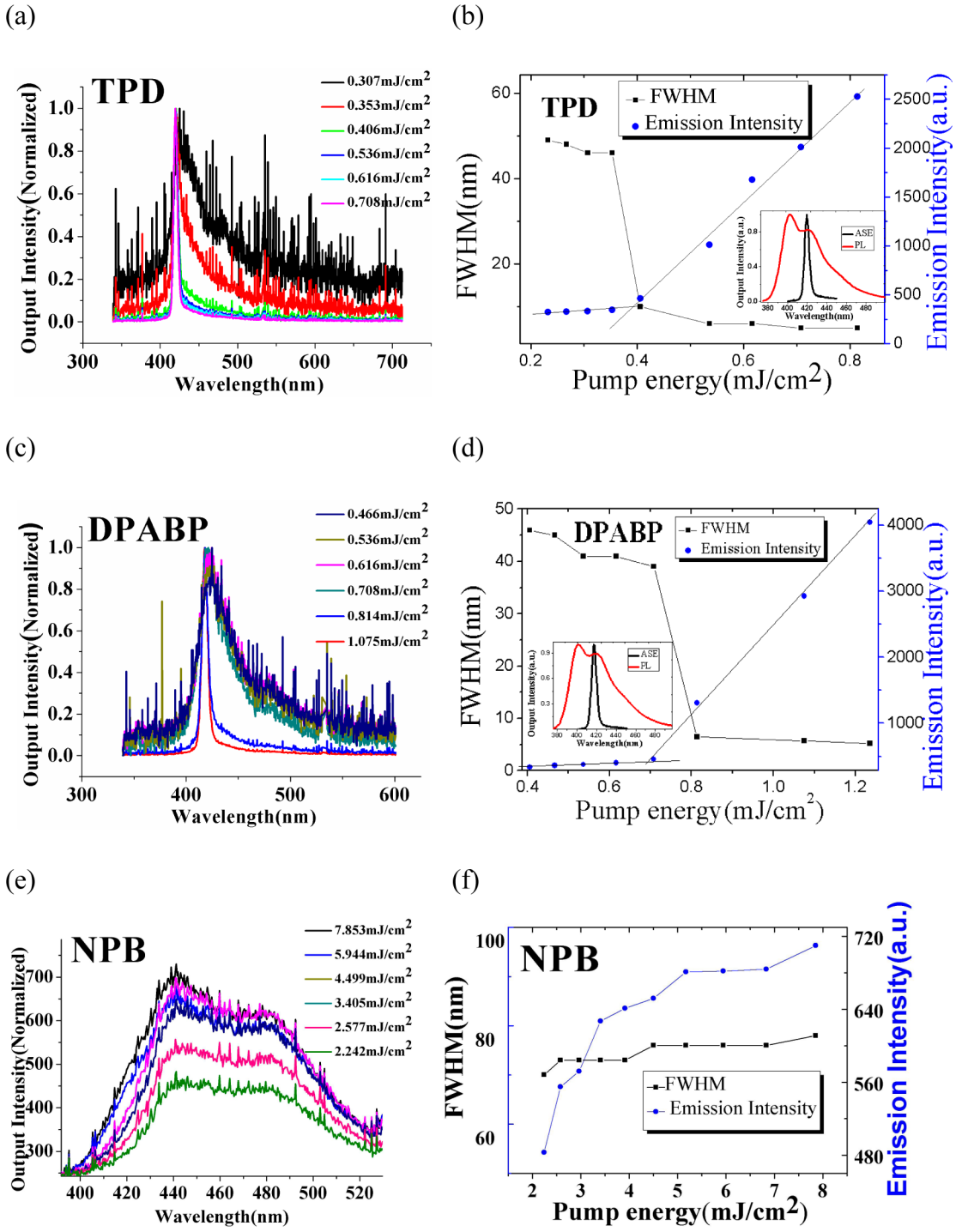

Figure 4. ASE characteristics of TPD, DPABP, and NPB. PL spectra of TPD (a), DPABP (c), and NPB (e) collected from the edge of the sample under laser pumped by different energy (355 nm); full widths at half-maximum (fwhm) and light emission peak intensity of TPD (b), DPABP (d), and NPB (f).

electronic transition dipole. The Franck–Condon factor can be expressed by a Poisson distribution:

$$|\langle 0_e|n_g\rangle|^2 = \frac{S^n}{n!}e^{-s} \tag{1-2}$$

In the Poisson distribution over the vibronic levels, S is Huang–Rhys factor, which represents the vibronic coupling strength:

$$S_j = \frac{\omega(\Delta Q_j)^2}{2\hbar} \tag{1-3}$$

Table 1. FWHM, ASE Threshold, λ_{ASE}, of Three Samples

sample	fwhm (nm)	ASE threshold (mJ/cm^2)	λ_{ASE} (nm)
sample 1: TPD	5.07	0.37	421.2
sample 2: DPABP	5.25	0.76	420.4
sample 3: NPB			

where ΔQ_j represents the displacement along the normal mode $(NM)_j$ between the equilibrium positions of the two electronic states. It is important to express the elongation ΔQ_j between the potential

dx.doi.org/10.1021/jp405692c | J. Phys. Chem. A 2013, 117, 10903−10911

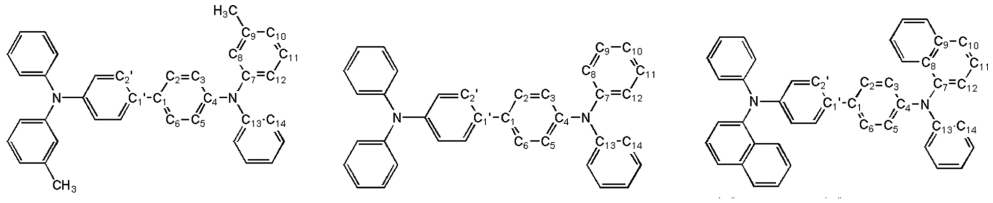

Figure 5. Molecular structures of *trans*-TPD, -DPABP, and -NPB.

Table 2. Optimized Geometries Parameters of the Trans Isomers of TPD, NPB, and DPABP

	TPD			DPABP			NPB		
	ground state[a]	excited state[b]	displacement[c]	ground state[a]	excited state[b]	displacement[c]	ground state[a]	excited state[b]	displacement[c]
$C_1-C'_1$	1.482 Å	1.440 Å	0.042 Å	1.482 Å	1.440 Å	0.042 Å	1.482 Å	1.449 Å	0.033 Å
C_1-C_2	1.406 Å	1.436 Å	−0.030 Å	1.406 Å	1.436 Å	−0.030 Å	1.405 Å	1.420 Å	−0.015 Å
C_4-N	1.419 Å	1.430 Å	−0.011 Å	1.420 Å	1.430 Å	−0.010 Å	1.421 Å	1.389 Å	0.032 Å
$C_{11}-C_{12}$	1.393 Å	1.390 Å	0.003 Å	1.393 Å	1.390 Å	0.003 Å	1.412 Å	1.412 Å	0 Å
C_8-C_9	1.393 Å	1.390 Å	0.003 Å	1.393 Å	1.390 Å	0.003 Å	1.435 Å	1.435 Å	0 Å
$C_{13}-C_{14}$	1.404 Å	1.411 Å	−0.007 Å	1.404 Å	1.411 Å	−0.007 Å	1.404 Å	1.401 Å	0.003 Å
$C'_2-C'_1-C_1-C_2$	35.0°	10.9°	24.1°	35.8°	10.8°	25.0°	35.3°	17.3°	17.9°
$C_3-C_4-N-C_7$	40.1°	53.4°	−13.3°	41.0°	53.2°	−12.2°	43.9°	−17.2°	61.1°
$C_5-C_4-N-C_{13}$	40.0°	53.5°	−13.5°	41.0°	53.2°	−12.2°	32.9°	−24.2°	57.1°

[a]The electronic ground-state. [b]The first excited-state. [c]The change between two geometries is displacement.

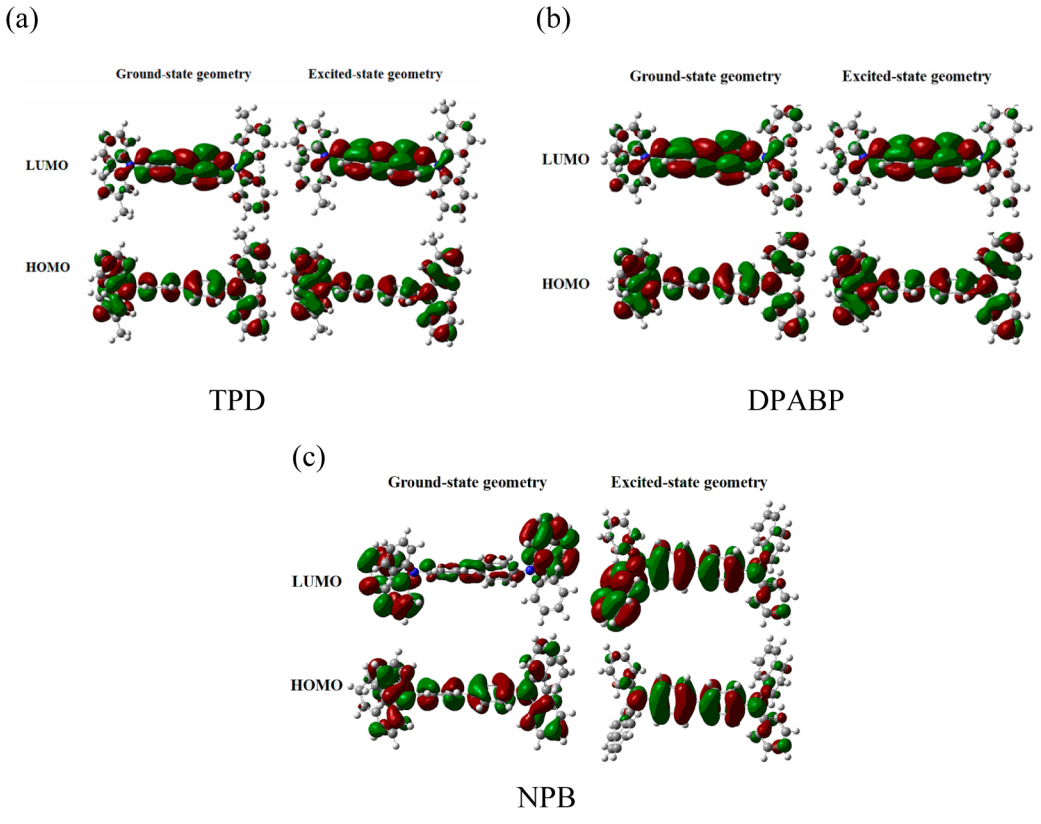

Figure 6. Frontier molecular orbital in the ground-state geometry and first exited-state geometry of TPD (a), DPABP (b), and NPB (c).

energy surface (PES) of the ground-state and first excited-state for each mode $\hbar\omega$ in terms of a dimensionless constant S:

$$\Delta Q_j = L_j \Delta q \tag{1-4}$$

$$\Delta q_j = m^{1/2} \Delta x \tag{1-5}$$

$$\Delta x = x_g - x_e \tag{1-6}$$

where L_j is vibrational eigenvector of the jth frequency mode;[20] m is single atomic mass; x_g and x_e are atomic Cartesian coordinate for ground state and excited state, respectively.

3.2. Results and Discussion. *3.2.1. Optimized Geometries and Frontier Molecular Orbital.* In order to obtain the

dx.doi.org/10.1021/jp405692c | J. Phys. Chem. A 2013, 117, 10903−10911

Table 3. Schedule of the Specific Parameters of the Most Strongly Elongated Internal Modes

	TD-DFT								
	TPD			DPABP			NPB		
B3LYP $h\omega$	$h\omega_j$[a] (cm^{-1})	S_j[b] (1)	λ_j[c] (cm^{-1})	$h\omega_j$[a] (cm^{-1})	S_j[b] (1)	λ_j[c] (cm^{-1})	$h\omega_j$[a] (cm^{-1})	S_j[b] (1)	λ_j[c] (cm^{-1})
low-frequency modes (0−200 cm^{-1})	23	0.202	4.7				9	26.901	230.6
	31	1.76	54.1	52	8.959	465.4	13	1.743	22.5
	36	3.333	118.8	68	1.784	120.9	22	4.725	102.6
	43	0.335	14.2	98	2.914	286.8	25	6.827	169.4
	49	5.498	271.9				31	3.952	124.2
	66	1.072	70.9				38	9.305	350.5
	87	0.155	13.6				46	3.467	160.3
	95	3.564	340.2				51	0.863	43.9
							56	3.211	180.3
							77	1.021	78.9
							93	0.308	28.8
							102	0.142	14.5
							123	0.923	113.3
							156	0.215	33.3
							172	0.151	26
							185	0.247	45.7
low-frequency modes (200−800 cm^{-1})							295	0.067	19.7
							424	0.066	27.8
				318	0.056	17.9	429	0.061	26.4
	426	0.119	50.6	427	0.15	64	486	0.068	33.4
	780	0.072	56.2	536	0.067	35.8	513	0.059	30.4
				786	0.101	79.6	527	0.090	47.7
							535	0.094	50.5
							550	0.073	40.3
high-frequency modes (1000−1700 cm^{-1})							1216	0.115	139.5
	1309	0.051	66.4	1199	0.059	70.9	1318	0.065	85.7
	1564	0.053	83.2	1310	0.071	93.8	1336	0.118	157.7
	1651	0.012	20.6	1320	0.053	69.7	1406	0.326	458.9
	1654	0.07	115.3	1653	0.071	116.8	1625	0.058	94.5
	1664	0.151	251.6	1664	0.166	277.5	1652	0.074	122.6
							1661	0.122	203.4

[a]Frequency modes. [b]Huang−Rhys factors (exceeds 0.05). [c]Reorganization energies.

molecular geometry in gas-phase, the optimized molecular geometries of the ground and first excited states were calculated. Figure 5 shows molecular structures of the trans-isomers of TPD, DPABP, and NPB. Only trans-isomer has been investigated because cis−trans isomerization did not induce major changes in the electronic transition energies and vibronic energies.[11] The detailed geometric parameters are shown in Table 2. For the trans-isomer TPD, which the methyls are in the opposite directions, a few works about the theory analysis were published.[11,17,19] Our results are in good agreement with those reported previously by others.[11] Moreover, Kennedy[17] has confirmed that the value of the central torsion angle of crystal TPD molecule is −34.7 (5)°, which is in good agreement with our calculation (Table 2). However, the calculated equilibrium molecule deviates to some extent from the crystal structure.[18] In the crystalline phase, as obtained by X-ray diffraction measurements on single crystals, the peripheral wings adopt considerably different conformations, thus breaking the C_2 symmetry that the free molecule can realize. For these molecules, the molecular equilibrium geometry were obtained using C_2 symmetry constraints starting from a structure that corresponds to the global energy minimum. The structure of the trans-isomer TPD tends to be planar when the molecule is excited, with the central torsion angle reduced to 10.9°. The change in the torsion angle in the center of the molecule can be understood from the patterns of the orbitals shown in the Figure 6a,b. As for DPABP, when compared to TPD, it showed similar results for the torsion angles and bond length. This confirmed that removing the two methyls has little influence on the molecular geometry of DPABP.

Even though TPD and NPB have similar molecular structures, their optimized geometries are apparently different. Trans-isomer of NPB consists of a central biphenyl core and two twisted terminal naphthyl. The twisting in the ground state is quite pronounced, for example, the central torsion angle has a large value. It is shown that the torsion angles of the terminal rings are apparently different (43.9°, 32.9°), which is mainly because naphthyl produces the big spatial steric hindrance (Table 2). When excited, the torsion angle of the terminal rings decrease to −17.2° and −24.2°, respectively, which is different from TPD and DPABP. However, the central dihedral angle decreased from 35.3° to 17.3°. NPB also displays large geometry relaxations with changes in average C−C bond lengths of about 0.033 Å, while for TPD and DPABP, the average change in C−C bond lengths are 0.0158 and 0.0148 Å, respectively (Table 2).

Molecular structures directly influence the frontier molecular orbital (FMO); hence, TPD, DPABP, and NPB have difference in FMO. Comparing the FMO between the ground-state geometry and the first excited-state geometry of TPD and DPABP, both the HOMO and LUMO are mainly localized in the biphenyl core, and the LUMO in the excited state spreads less

dx.doi.org/10.1021/jp405692c | J. Phys. Chem. A 2013, 117, 10903−10911

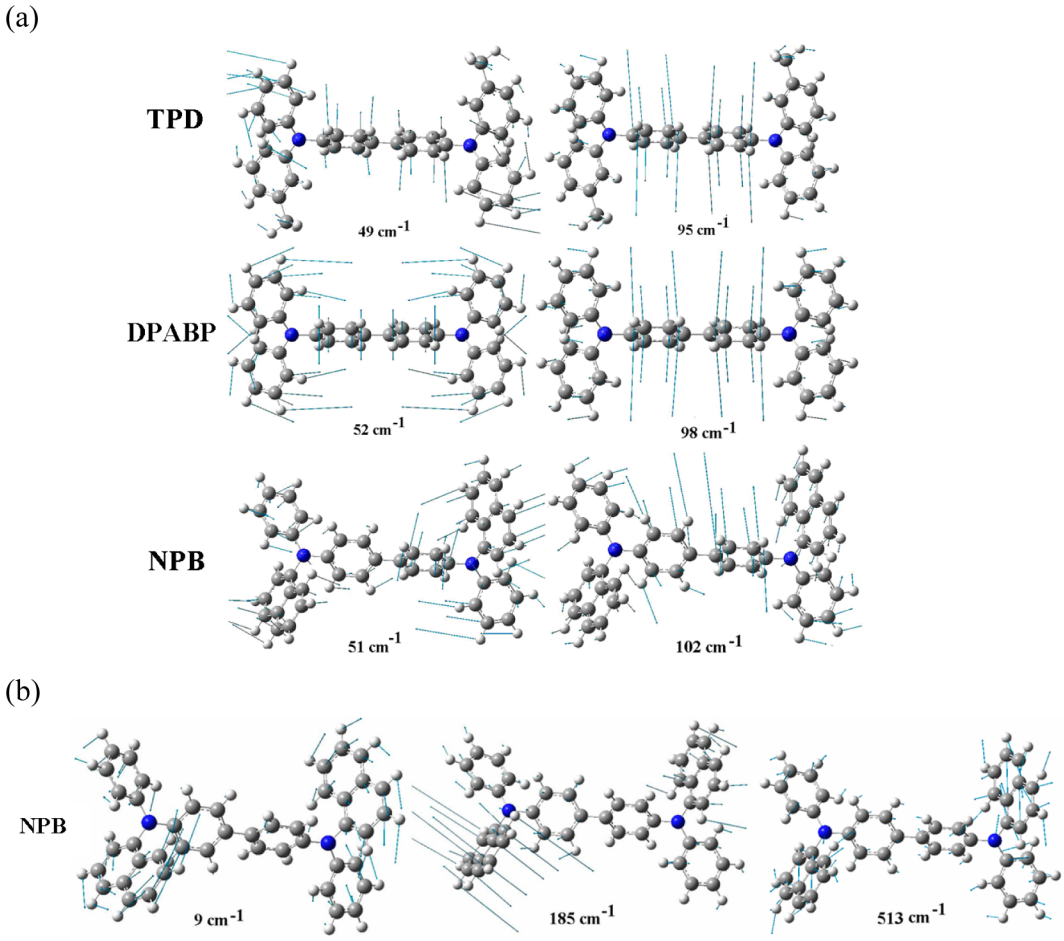

Figure 7. Calculated vibrational eigenvectors of dominating low-frequency modes: (a) the similar low-frequency modes for TPD, DPABP, and NPB; (b) the particular low-frequency modes for NPB. The contribution of each mode to the total deformation of samples is enlarged by the same factor.

over the peripheral phenyl groups; the DFT calculations showed that molecular structures of TPD and DPABP have relatively small change (detail in Table 2), especially in geometric changes of the central core and bond lengths. However, NPB exhibited considerable change, especially in LUMO. In the ground state, the LUMO spreads less over the central biphenyl core than peripheral naphthyl group since the large torsion angles at the center (35.3°) precluded the coplanarity. When excited, NPB becomes nearly planar (the central angle is about 17.3°), the LUMO spreads much more over the central biphenyl core.

3.2.2. Vibrational Modes. From the optimized molecular geometries, the relative parameters of vibrational modes can be calculated by Franck−Condon approximation, and a projection on the internal vibrations due to eigenvectors of the vibrational modes L_j and the deformation patterns Δq can be extracted. As shown in the eqs from 1-1−1-3 to 1-1−1-6, the electron-vibration constant S is proportional to the square of NM displacements. Hence, it can be concluded that the strength of electron-vibration is related to both L_j and Δq.

In low-frequency modes, according to Franck−Condon principle (eqs 1-1−1-3), TPD and DPABP have the weak and a little number of low-frequency internal vibrations because of their relative small deformation patterns Δq and little strong vibrational eigenvectors L_j than NPB. Hence, as shown in Table 3, calculation results show that TPD and DPABP have a smaller number of vibrational modes than NPB, especially below 800 cm^{-1}. The numbers of the strong low-frequency modes of TPD, DPABP, and NPB are 10, 7, and 24, respectively, and all of the modes are torsional modes.[21] Figure 7 shows the typical vibrational eigenvectors in low vibrational modes below 200 cm^{-1} of the three molecules. TPD, DPABP, and NPB have several similar modes. They all have out-of-plane C−C torsional modes within the whole molecule and torsional modes arising form central biphenyl core (see Figure 7a). However, as shown in Figure 7b, NPB has a large amount of C−C swing vibration modes mainly arising from two twisted terminal naphthyl group, which result in more low-frequency modes than TPD and DPABP. More low-frequency will influence the shape of PL spectra and the formation of energy level system.

In high-frequency modes (1000−1700 cm^{-1}), all of three molecules have strong elongation mode (Table 3). The internal vibrations of high-frequency modes and low-frequency modes contribute to the first vibronic subband of PL spectra, the elongation of low-frequency modes results in a broadening of the vibronic subbands defined by the high-frequency modes.[11,20,22] For TPD and DPABP, distinct vibronic sidebands are obtained in PL spectra, and ASE occurs at this sideband. However, there is only a weak visible subband in NPB because of more low-frequency modes even though there are strong internal vibrations in high-frequency modes.

The calculated total reorganization energies of TPD, DPABP, and NPB are 0.566, 0.565, and 1.058 eV, respectively, according to the third column in Table 3. These calculation results are in good agreement with the experimental Stokes shift (0.426 , 0.418, and 0.744 eV) because the inner reorganization energies λ play a crucial role in the interpretation of the Stokes shift.[11,22] For

dx.doi.org/10.1021/jp405692c | J. Phys. Chem. A 2013, 117, 10903−10911

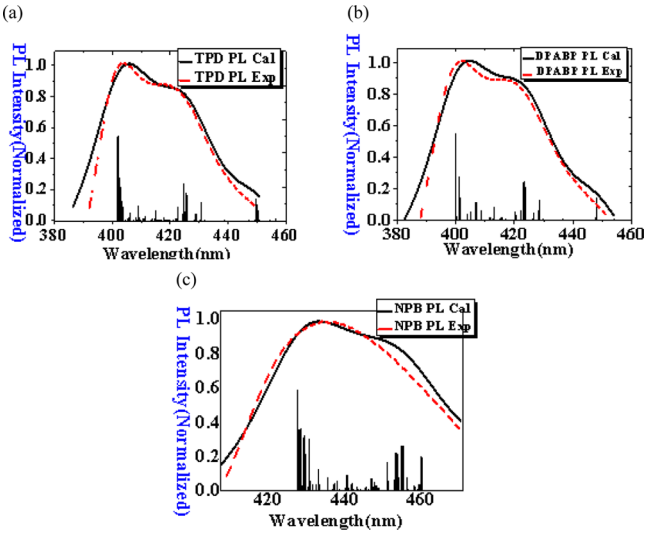

Figure 8. Model simulation (red solid lines) of the linear PL of TPD, DPABP, and NPB molecules based on the product of the Poisson distributions of the internal vibration according to the elongations calculated with DFT referred to Table 3 and refs 19 and 21. Discrete vertical bars, normalized to the height of the main peak at 3.08 eV (a), 3.10 eV (b), and 2.95 eV (c), respectively, isare discrete vibronic transitions. The experiment PL spectra (black solid line) are measured by three samples.

TPD and DPABP, Table 3 shows that reorganization energies of low-frequency normal modes mainly contribute to the total reorganization energy. However, for NPB, the total reorganization energy is due to both reorganization energies of low-frequency modes and high-frequency modes.

3.2.3. PL Spectra. According to the analysis of vertical transition energy and the relative parameters of vibrational modes, the PL spectra can be calculated. The various discrete vibronic transitions were calculated using vibrational progressions, which are related to Huang–Rhys factors S_j.[23−25] In the fitting procedure, fwhm were optimized in order to minimize the sum of the squares of the deviations between experimental and computed spectra. It was shown that the fitting was with a suitable Lorentzian broadening of fwhm = 0.093 eV, which was adjusted manually to match the corresponding experimental spectra.

For TPD (Figure 8a), the lowest transition energy for the excited-state geometry calculated at the B3LYP/6-31d(d,p) level is 2.89 eV, which is only about 0.2 eV below the maximum of the measured PL. The calculated PL spectrum is in excellent agreement with the experimental PL spectrum, for the main peak and first subband. The different discrete levels merge into a large band (around 404 nm) and two apparent sidebands (around 424 and 454 nm). It can be concluded that the relative small number of torsional modes (11−689 cm^{-1}) of TPD result in a relative small broadening in PL spectrum line width, so there are obvious peaks in PL spectrum. Similar calculations performed on DPABP elucidated similar results (in Figure 8b). However, for NPB, the calculated vertical transition energy is 2.84 eV, which is only about 0.2 eV below the maximum of the measured PL peak. Shown in Figure 8c, NPB has a main peak in 433 nm and only weak visible subbands; a greater quantity of discrete vibronic levels deriving from low-frequency modes exist between them. Since NPB has a large number of strong low-frequency internal modes, the PL line shape of NPB is then strongly broadened.

3.2.4. Four-Level System. The discrete vibronic transitions in PL spectrum exhibited different energy levels in the ground state (Figure 9). Figure 9 shows the energy levels of both the ground and the first excited singlet states. In each state, the electronic level is divided into vibronic sublevels. The spacing of these sublevels is approximately 0.15 eV, so there is little thermal excitation from the lowest level at room temperature.

For example, for TPD, the spacing of sublevels from the main peak and the first vibronic subband is 0.144 eV (from 404 to 424 nm). A small number of low-frequency modes corresponding to distinct sideband result in the clear energy level structure. When samples were photopumped, pump laser can excite the molecule from its ground state to an excited vibrational level vertically, usually the first excited singlet state, which will be followed by rapid thermal relaxation to the bottom of the excited singlet state. Because of TPD and DPABP, lasing can take place via the transition from the lowest excited singlet state to the first vibronic sublevel of ground state, which is followed by rapid relaxation to the bottom of the ground state. The thermal relaxtion rate (~10^{-12}−10^{-10} s) within the vibronic manifold is faster than the emission process (~10^{-10}−10^{-7} s).[26] Hence, the energy levels of these organic semiconductors enable them to behave as a four-level system with population inversion between v_0'' and v_1', even when most molecules are in the ground state, so

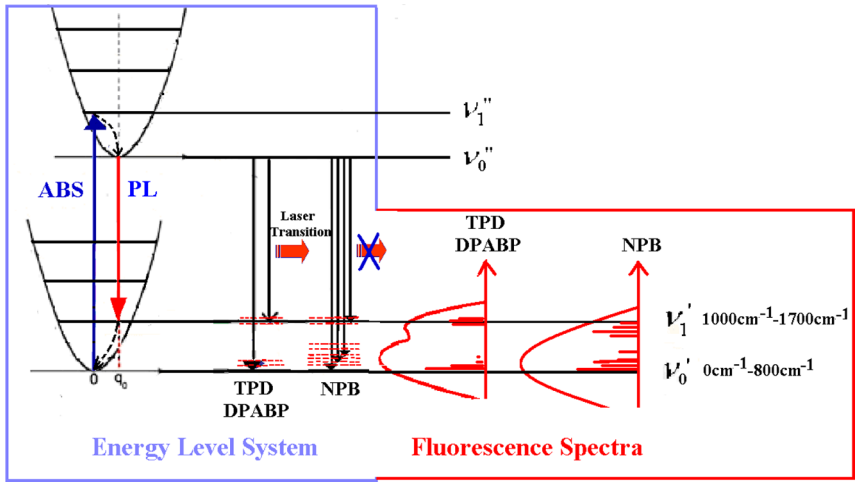

Figure 9. Energy level difference of TPD, DPABP, and NPB reflected from the relation between the optical spectra and vibronic levels. TPD and DPABP have an effective four-level system.

dx.doi.org/10.1021/jp405692c | J. Phys. Chem. A 2013, 117, 10903−10911

lasing can be obtained for a very low rate of excitation, that is the low threshold for lasing. The four-level system also explains why the emission occurs at longer wavelength than the absorption.

However, as for NPB, the spacing of sublevels between υ_1' and υ_0' contains segments with a range of consecutive energy levels, which result from a large number of strong low-frequency torsional modes. As discussed in section 3.2.2, these strong elongated low-frequency modes of NPB are relative with large displacements ΔQ in low-frequency modes, as shown in eqs 1-1−1-3. Therefore, for NPB, only a small number of molecules undergo rapid relaxation to the bottom of the ground state after the transition from the lowest excited singlet state to the first vibronic sublevel of ground state because a series of energy levels exist between υ_1' and υ_0', so an effective four-level system will not be formed; hence, it can neither form a higher population inversion between υ_0'' and υ_1' nor gain an efficient stimulated amplification.

4. CONCLUSIONS

In conclusion, it was shown that TPD and DPABP exhibited significant ASE at the first subband of PL spectra in optically pumped polystyrene (PS) films, and there was no significant gain-narrowing in NPB even at a high pump energy. On the basis of DFT and Franck−Condon principle, we have shown that the most strongly elongated high-frequency modes contribute to the first vibronic sublevels of ground state, which can be also observed in PL spectra (the subbands). Hence, TPD and DPABP furnished significant subbands in PL spectrum, but NPB did not. Moreover, the less elongated low-frequency modes make TPD and DPABP produce an appreciable energy gap between the bottom and the first vibronic sublevel of ground state, which can form an effective four-level system and population inversion. However, for NPB, relatively more low-frequency modes contributing to a range of consecutive energy levels lead to an unclear energy gap, which destroys the formation of a four-level system. It is the unique molecular geometry of TPD and DPABP that is suitable to form a four-level system and population inversion for lasing.

As we know, this is the first time anyone has provided a valuable approach to better understanding of the microscopic interpretation of laser action in organic lasers materials and a screening model to guide the design for more efficient novel lasing materials.

AUTHOR INFORMATION

Corresponding Authors

*(Z.W.) E-mail: zhaoxinwu@mail.xjtu.edu.cn. Tel: +86-29-82664867. Fax: +86-29-82664867.

*(X.Z.) E-mail: xzhao@mail.xjtu.edu.cn. Tel: +86-29-82665671. Fax: +86-29-82668559.

Notes

The authors declare no competing financial interest.

ACKNOWLEDGMENTS

This work was financially supported by Basic Research Program of China (2013CB328705), National Natural Science Foundation of China (Grant Nos. 61275034 and 61106123), Fundamental Research Funds for the Central Universities (Grant No. xjj2012087), and China Postdoctoral Science Foundation (Grant No. 20110491653).

REFERENCES

(1) McGehee, M. D.; Heeger, A. J. Semiconducting (conjugated) polymers as materials for solid-state lasers. *Adv. Mater.* **2000**, *12*, 1655−1668.

(2) Samuel, I. D. W.; Turnbull, G. A. Organic semiconductor lasers. *Chem. Rev.* **2007**, *107*, 1272−1295.

(3) Zapka, W.; Brackmann, U. Shorter dye laser wavelengths from substituted *p*-terphenyls. *Appl. Phys.* **1979**, *20*, 283−286.

(4) Haghighi, H. R.; Forget, S.; Chénais, S.; Siove, A.; Castex, M. Laser operation in nondoped thin films made of a small-molecule organic red-emitter. *Appl. Phys. Lett.* **2009**, *95*, 033305.

(5) Ma, S. Y.; Nakajima, T.; Yamashita, K. Solid state organic laser emission at 970 nm from dye-doped fluorinated-polyimide planar waveguides. *Appl. Phys. Lett.* **2008**, *93*, 023306.

(6) Tsiminis, G.; Wang, Y.; Shaw, P. E.; Kanibolotsky, A. L.; Perepichka, I. F.; Dawson, M. D.; Skabara, P. J.; Turnbull, G. A. Low-threshold organic laser based on an oligofluorene truxene with low optical losses. *Appl. Phys. Lett.* **2009**, *94*, 243304.

(7) Calzado, E. M.; Villalvilla, J. M. Concentration dependence of amplified spontaneous emission in organic-based waveguides. *Org. Electron.* **2006**, *7*, 319−329.

(8) Salbeck, J. N.; Bauer, J.; Weissortel, F.; Broms, P.; Andersson, A.; Salaneck, W. R. Solid state amplified spontaneous emission in some Spiro-type molecules: A new concept for the design of solid state lasing molecules. *Synth. Met.* **1999**, *101*, 405−408.

(9) Schneider, D.; Rabe, T.; Riedl, T.; Dobbertin, T.; Werner, O. Deep blue widely tunable organic solid-state laser based on a spirobifluorene derivative. *Appl. Phys. Lett.* **2004**, *84*, 4693−4695.

(10) Anni, M.; Gigli, G.; Cingolani, R.; Rossi, M. Z.; Gadermaier, C.; Lanzani, G.; Barbarella, G.; Favaretto, L. Amplified spontaneous emission from a soluble thiophene-based oligomer. *Appl. Phys. Lett.* **2001**, *78*, 2679−2681.

(11) Scholz, R.; Gisslén, L.; Himcinschi, C.; Vragovic, I.; Calzado, E. M.; Louis, E.; San Fabian, E.; Díaz-García, M. A. Asymmetry between absorption and photoluminescence line shapes of TPD: spectroscopic fingerprint of the twisted biphenyl core. *J. Phys. Chem. A* **2009**, *113*, 315−324.

(12) Holzer, W.; Penzkofer, A.; Hörhold, H. H. Travelling-wave lasing of TPD solutions and neat films. *Synth. Met.* **2000**, *113*, 281−287.

(13) Kawamura, Y.; Yamamoto, H.; Goushi, K.; Sasabe, H.; Adachi, C. Ultraviolet amplified spontaneous emission from thin films of 4,4′-bis(9-carbazolyl)-2,2′-biphenyl and the derivatives. *Appl. Phys. Lett.* **2004**, *84*, 2724−2726.

(14) Díaz-García, M. A.; Avila, S. F. D.; Kuzyk, M. D. Dye-doped polymers for blue organic diode lasers. *Appl. Phys. Lett.* **2002**, *80*, 4486−4488.

(15) Gehee, M. M.; Gupta, R.; Veenstra, S.; Miller, E. K.; Diaz-Garcia, M. A.; Heeger, A. J. Amplified spontaneous emission from photo-pumped films of a conjugated polymer. *Phys. Rev. B* **1998**, *58*, 7035−7039.

(16) Calzado, E. M.; Villalvilla, J. M.; Boj, P. G.; Quintana, J. A. Tuneability of amplified spontaneous emission through control of the thickness in organic-based waveguides. *J. Appl. Phys.* **2005**, *97*, 093103.

(17) Kennedy, A. R.; Smith, W. E.; Tackley, D. R.; David, W. I. F.; Shankland, K.; Brown, K. Tetraaryl biphenyl diamine hole transport materials: a structural study utilizing both single crystal and high resolution powder diffraction. *J. Mater. Chem.* **2002**, *12*, 168−172.

(18) Zou, L. Y.; Ren, A. M.; Feng, J. K.; Ran, X. Q. Theoretical design study on multifunctional triphenyl amino-based derivatives for OLEDs. *J. Phys. Org. Chem.* **2009**, *22*, 1104−1113.

(19) Vragovic, I.; Scholz, R.; Schreiber, M. Model calculation of the optical properties of 3,4,9,10-perylene-tetracarboxylic-dianhydride (PTCDA) thin films. *Europhys. Lett.* **2002**, *57*, 288−294.

(20) Scholz, R.; Kobitski, A. Y.; Kampen, T. U.; Schreiber, M.; Zahn, D. R. T. Resonant Raman spectroscopy of 3,4,9,10-perylene-tetracarboxylic-dianhydride epitaxial films. *Phys. Rev. B* **2000**, *61*, 13659−13669.

(21) Scholz, R.; Schreiber, M. Linear optical properties of perylene-based chromophores. *Chem. Phys.* **2006**, *325*, 9−21.

(22) Vragovic, I.; Calzado, E. M.; Díaz-García, M. A. The structure and energetics of TPD ground and excited states. *Chem. Phys.* **2007**, *332*, 48−54.
(23) Peeters, E.; Ramos, A. M.; Meskers, S. C. J.; Janssen, R. A. J. Singlet and triplet excitations of chiral dialkoxy-*p*-phenylene vinylene oligomers. *J. Chem. Phys.* **2000**, *112*, 9445−9454.
(24) Peng, Q.; Yi, Y.; Shuai, Z.; Shao, J. Toward quantitative prediction of molecular fluorescence quantum efficiency: role of duschinsky rotation. *J. Am. Chem. Soc.* **2007**, *129*, 9333−9339.
(25) Gruhn, N. E.; da Silva Filho, D. A.; Bill, T. G.; Malagoli, M.; Coropceanu, V.; Kahn, A.; Brédas, J.-L. The vibrational reorganization energy in pentacene: molecular influences on charge transport. *J. Am. Chem. Soc.* **2002**, *124*, 7918−7919.
(26) Valeur, B. Molecular Fluorescence: Principles and Applications. In *Characteristics of Fluorescence Emission*; Wiley VCH: Weinheim, Germany, 2002; Chapter 3, p 35.